IEEE Access
Multidisciplinary ⋮ Rapid Review ⋮ Open Access Journal

Received 3 July 2025, accepted 26 August 2025, date of publication 28 August 2025, date of current version 9 September 2025.

Digital Object Identifier 10.1109/ACCESS.2025.3603958

RESEARCH ARTICLE

MonolayerFFF: An Image Dataset of MonolayerFFF 3D Printed Parts With Different Fabrication Conditions

THIAGO G. LOPES[1,2], PAULO M. C. MONSON[1], PAULO R. AGUIAR[3], DORIANA M. D'ADDONA[2], AND PEDRO O. C. JÚNIOR[1], (Senior Member, IEEE)

[1]Department of Electrical and Computer Engineering, São Carlos School of Engineering, University of São Paulo, São Carlos 13566-590, Brazil
[2]Department of Chemical, Materials and Industrial Production Engineering, University of Naples Federico II, 80125 Napoli, Italy
[3]Department of Electrical Engineering, São Paulo State University, Bauru 17033-360, Brazil

Corresponding author: Pedro O. C. Júnior (pedro.oliveiracjr@usp.br)

This work was supported in part by the CAPES—Coordenação de Aperfeiçoamento de Pessoal de Nível Superior-Brasil (Code 001), through the Programa de Doutorado Sanduíche no Exterior (PDSE), under Grant 88881.846265/2023-01 and Grant 88887.666942/2022-00; and in part by the National Council for Scientific and Technological Development (CNPq) under Grant 306774/2021-6 and Grant 445054/2024-7.

ABSTRACT This research presents the MonolayerFFF dataset, a novel addition to Fused Filament Fabrication (FFF) 3D printing image-based datasets, focusing on monolayer parts with unique geometric variations. Unlike existing multi-layered datasets, MonolayerFFF comprises three specific monolayer part conditions: Regular, Defect 1 (with reduced filament deposition), and Defect 2 (featuring filament retraction). This approach offers a different perspective on 3D printing analysis, capturing a range of typical and atypical scenarios. Utilizing the GoogLeNet architecture for Convolutional Neural Network (CNN) classification, the study achieved a notable validation accuracy of 95.81% on the MonolayerFFF dataset, demonstrating its quality and diversity without relying on data augmentation. The high accuracy, coupled with minimal misclassifications as evidenced in both test and validation confusion matrices, underscores the effectiveness of the proposed backbone for feature extraction and classification in identifying subtle differences in part conditions. The study's outcomes, including the absence of overfitting and aligned loss curves, highlight the model's capability to generalize from training to unseen data. The MonolayerFFF dataset, with its focus on monolayer parts and detailed variation in conditions, emerges as a significant contribution to advancing CNN analysis in the field of 3D printing. Its potential for real-time monitoring and quality assurance in additive manufacturing promises to enhance the FFF process efficiency and accuracy, making it a valuable tool for researchers in the field.

INDEX TERMS Image dataset, fused filament fabrication, monolayer, convolutional neural networks, machine learning.

I. INTRODUCTION

The Additive Manufacturing (AM) process known as Fused Deposition Modeling (FDM) was developed in the 1980s by S. Scott Crump, co-founder of Stratasys. This technology utilizes a thermoplastic filament that is extruded through a heated nozzle and deposited layer by layer to fabricate a three-dimensional object [1]. Initially, FDM was patented by Stratasys, which restricted its commercial application to the company's products and systems. During the term of the patent, FDM became one of the most recognized 3D printing technologies, particularly for industrial applications and rapid prototyping [1], [2]. Following the expiration of the FDM patent in 2009, the 3D printing community adopted the term Fused Filament Fabrication (FFF) to refer to the same process [3]. In the FFF process, filament deposition is achieved by the movement of either the extruder or the printing bed, as illustrated in Fig. 1.

The associate editor coordinating the review of this manuscript and approving it for publication was Vishal Srivastava.

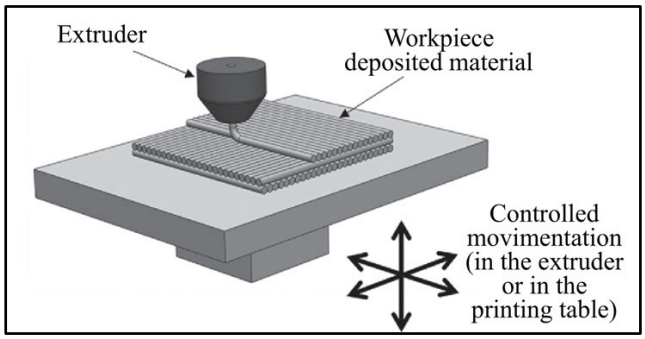

FIGURE 1. Representation of the movement of the workpiece or of the extruder, necessary for the filament deposition in the FDM process [8].

As the base for all subsequent layers, the fabrication of the first layer is of critical importance [4]. Several studies have addressed this topic, focusing on process monitoring and defect detection [5], [6], [7].

Undesired variations in the final properties of printed parts may appear as anomalies in fundamental layer parameters [8] or as geometric discrepancies between the idealized model and the printed part [9].

Damage to parts during the FFF AM process can lead to significant costs and losses due to the high added value of these components. The most frequent types of damage in the FFF process include delamination or detachment of the first layer from the print bed, surface scratching by the extruder, filament shrinkage, under-extrusion, geometric deviations from the idealized model, warping at the part edges, partial or full nozzle clogging, and filament runout in the extruder [10], [11], [12], [13].

As discussed by [14], there are generally two categories of quality monitoring for the FFF process: (1) monitoring of the printer's health status, and (2) detection of product defects during printing. In both cases, effective FFF process monitoring requires real-time measurement and analysis of various process parameters.

The monitoring of manufacturing processes can be achieved in many ways. One such approach is in-situ monitoring, where a sensor or other data collection device is placed directly at the site of the manufacturing process, in close proximity to the machine. In-situ monitoring is particularly valuable, as it provides real-time and reliable data captured directly from the process, enabling more accurate assessments of manufacturing conditions [15].

On this topic, the article developed by [14] performs a comprehensive literature analysis regarding the sensors and methods for the in-situ monitoring of the FFF process.

There are examples of authors who investigate in-situ monitoring by using instruments such as vibration sensors [11], [16], acoustic sensors [4], [6], and low-cost transducers [5], [7]. However, the FFF process in-situ monitoring can also be accomplished by the use of Machine Learning (ML) methods, as seen in the works [17], [18].

As stated by [19], one of the most established algorithms among various deep learning models is the convolutional neural network (CNN). The CNN is a class of artificial neural networks that has been a dominant method in computer vision tasks.

In the literature, there are examples of articles that go into the monitoring of defects in the FFF process by using CNN models. In one of these examples, the authors of [18] used a CNN classification model to monitor the warping defect in the FFF process through images collected by an optical camera. In order to train and validate the CNN model, the authors employed a private dataset consisting of 520 images. In another example, the authors of [20] employed a CNN classification model to monitor the occurrence of under-extrusion and over-extrusion in the part's surface through images collected by an optical camera attached to the 3D printer extruder block. In this article, the authors also employed a private dataset of FFF-produced parts' surface images in order to train and validate the CNN model.

In order to perform research into ML algorithms, such as CNN models, a dataset of some sort is necessary. The dataset used in the computer vision CNN research articles varies between private datasets, such as the ones used by [18] and [20], that in most cases are generated with the purpose of achieving a single research objective and are publicly available datasets.

There are many platforms, such as Mendeley Data and Zenodo, that serve as repositories for public image datasets that can be freely downloaded and used in computer vision CNN research. One of these datasets is [21], a dataset composed of breast ultrasonic images that show up as being cited by 694 articles by December 2023 in the Google Scholar indexing tool. There are many instances in the 694 articles that cited [21] which are studies that used the dataset as input for computer vision CNN research, which shows how much of an important role a publicly available image dataset plays in ML research.

The purpose of this research is to present the MonolayerFFF dataset with an application example of CNN classification. Our contributions can be summarized as follows:

1) We construct a new FFF image dataset called MonolayerFFF, which comprises 776 surface images that have been obtained from monolayer parts manufactured under one of three classes (two corresponding to region-specific induced printing defects and one corresponding to normal printing).
2) We validated the usability of the MonolayerFFF on research regarding the monitoring of defects in the FFF process through the use of CNN, by successfully classifying the printing defects with the well-established GoogLeNet architecture.

II. RELATED WORKS

Regarding related works, which similarly aim to introduce novel image datasets with examples of classification applications, an example is found in the work developed by [22]. In their study, [22] constructed the Laryngoscope8 dataset,

comprised of 3,057 laryngoscope images under eight labels (seven corresponding to laryngeal diseases and one for normal tissue), showcasing the use of the Laryngoscope8 dataset for training a CNN model to classify different types of laryngeal diseases. The authors employed the DenseNet-121 architecture as their classification model backbone and conducted comparative analysis with other architectures such as CheXNet, AG-CNN, and Inception_v3.

Another example of work is the article by [23], which introduced the ITD (Industrial Tools Detection) dataset, comprised of over 11,000 RGB images of 8 object categories, and encompassing 24 common industrial tools with multiple distinct views of each tool. The usability of the ITD dataset was demonstrated through the use of various object detection and classification algorithms, including CNNs like the Fast Region-based Convolutional Network (Faster R-CNN) and the Region Fully Convolutional Networks (R-FCN).

Publicly available image datasets for the FFF process exist as well. In line with the MonolayerFFF dataset, the [24] dataset consists of surface profile images from the FFF fabrication process. However, the [24] dataset includes images obtained through the fabrication of entire parts, that is, parts comprised of multiple layers, utilizing a non-contact laser scanner for surface acquisition. This dataset categorizes parts based on conditions into four categories: under printing, over printing, normal, and empty regions. Contrarily, the *MonolayerFFF* dataset focuses on monolayer parts classified under one of three classes (two corresponding to region-specific induced printing defects and one to normal printing), distinguishing itself by concentrating on monolayer parts and region-specific induced defects.

Another FFF image dataset is mentioned alongside the article [25], which is composed of surface images captured layer-wise during the FFF process using an optical camera. Similar to the previously discussed dataset, the *MonolayerFFF* dataset distinguishes itself from the dataset employed by [25] by providing surface images of monolayer parts under one of three classes (two for region-specific induced printing defects and one for normal printing), offering a focused lens on the nuances of monolayer part fabrication and defect classification.

III. MATERIAL AND METHODS

A. MONOLAYER PARTS FABRICATION

The monolayerFFF dataset is composed of surface images obtained from $25 \times 25 \times 0.4$mm rectangular shape monolayer parts, with three types of parts conditions: Regular (H) part, that is without any induced defect; Defect 1 (D1), which is a part with a reducing of the deposition of filament in a specific region of the external printing pattern of the part; Defect 2 (D2), which is a part with a retraction of the deposition of filament in the printing of the middle raster line of the part.

Both D1 and D2 are proposed to mimic the under-extrusion type of defect, which is a common issue in FFF process [26], and its impact on two regions of a printed part where different deposition movements were conducted.

The printing parameters adopted for the printing conditions were defined in the Simplify3D software by Simplify and are available textually in the G-Code files within the MonolayerFFF dataset.

To achieve the D1 printing condition, the G-Code regarding three specific lines of the outer perimeter and inner perimeter of the contour printing lines was altered, as shown by Fig. 2 in the lines commented with ''altered''. The alteration was done to reduce the amount of filament being deposited on the right side of the C1, C2, and C3 contour lines, as seen in Fig. 3, by 75% of the original amount.

FIGURE 2. Alterations to the G-Code made to generate the defects.

On the other hand, in order to achieve D2 printing condition, the G-Code regarding a specific line of the raster printing lines were altered, as shown by Fig. 2 in the line commented with ''altered''. The alteration was done to induce filament retraction during the middle raster line (R28) fabrication, as seen in Fig. 3.

The G-Code regarding the H, D1 and D2 conditions, obtained after the slicing process in the Simplify3D software for both printing approaches, is available within the MonolayerFFF dataset.

In order to print the parts that compose the monolayerFFF dataset, an A1V2 model 3D printer, manufactured by GTMax3D, was utilized. This printer possesses a printer table with a printing surface of 300×200mm, and a Hotend Allmetal Extruder. A 1.75mm diameter blue PLA filament, manufactured by 3DFila, was utilized in this work.

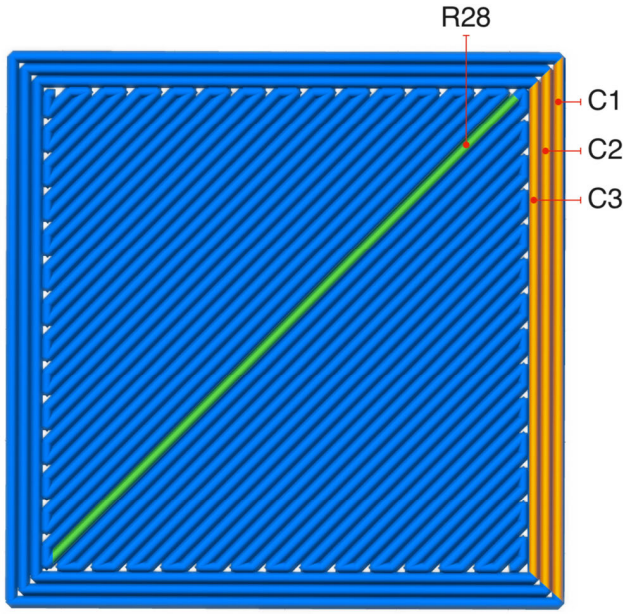

FIGURE 3. Lines identification.

Following the recommendation of the printer manufacturer for printing with PLA filament, before the printing of each batch of parts, 3 drops of machine oil were deposited on a small sponge attached to the filament infill of the 3D printer to avoid obstruction in the Hotend Allmetal Extruder.

The printing of the parts that compose the monolayerFFF dataset was performed at the Data Acquisition and Signal Processing laboratory of the São Paulo State University – Bauru Campus and was conducted with two printing approaches. The first printing approach was conducted with a reduced levelling area and printing area for the printing process. This was performed as a test to evaluate the impact of the reduced levelling area on the surface quality of the printing parts. In order to adjust the levelling area, a specific line of the part G-Code was altered. The inclusion of the 'P2 H40' instructions to the 268 code line, visually represented with orange characters in Fig4., reduced the levelling area to be closer to the geometric center of the printing table. On the other hand, the reduction of the available printing area was conducted manually, with the positioning of 28 copies of the monolayer model on the Simplify3D software representation of the A1V2 printing table, as can be seen in the upper representation of Fig. 6.

```
265 M402
266 G28; GENERAL HOME
267 M400
268 G29 V4 T ; AUTO LEVELLING
269 M400
270 M104 S180; PRE-HEAT THE EXTRUDER NOZZLE
```
Default

```
265 M402
266 G28; GENERAL HOME
267 M400
268 G29 P2 H40 V4 T ; AUTO LEVELLING ALTERED
269 M400
270 M104 S180; PRE-HEAT THE EXTRUDER NOZZLE
```
Reduced

FIGURE 4. Auto levelling code used in the Default and Reduced printing approaches.

The second printing approach was that of not any alteration of the auto levelling area, and with the positioning of 40 copies of the monolayer model on the Simplify3D software representation of the A1V2 printing table, as can be seen on the bottom representation of Fig. 6. A representation of a batch printed under the second printing approach is displayed on Fig. 5.

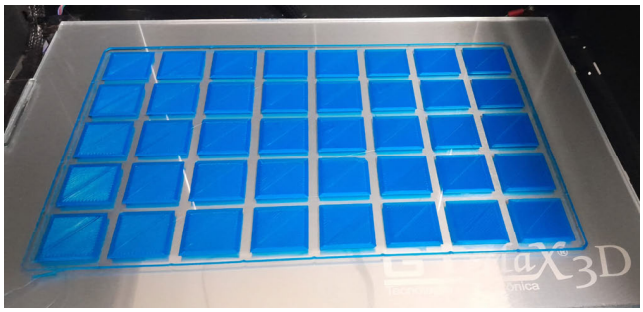

FIGURE 5. Printing batch.

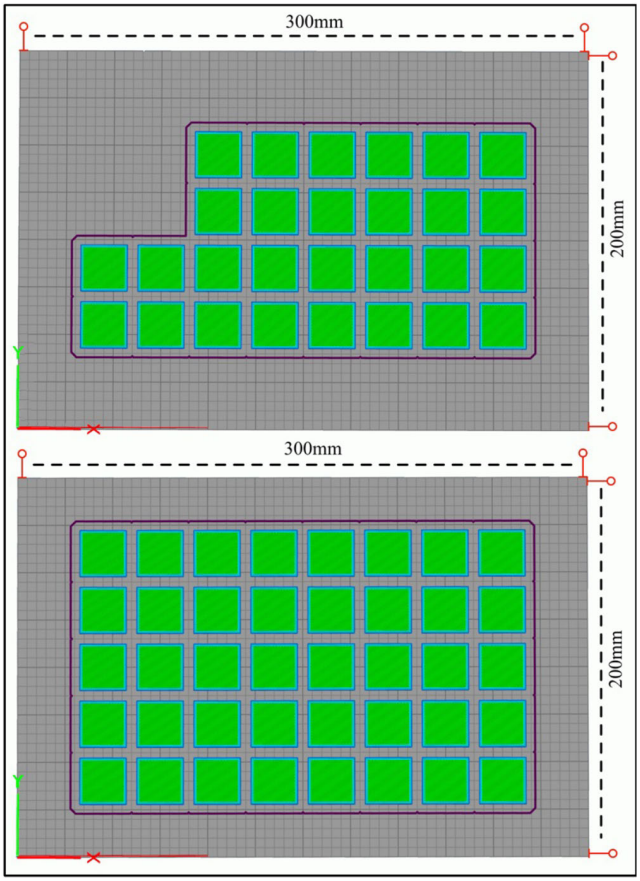

FIGURE 6. Sliced parts for both printing approaches.

The variation of the levelling area between the first and two printing approaches brought the introduction at of random small variations to the surface of the monolayer parts. These small variations are the result of miscalibration of the printer's internal surface map caused by the reduced levelling area. However, these aleatory variations did not significantly affect the regions of interest for the proposed defects. Thus, they were not further investigated in the present research but may be explored in future research.

B. DATASET PREPARATION

To scan the surface of the parts to compose the monolayerFFF image dataset, a LiDE 300 model scanner, manufactured by Canon, was employed. The monolayer parts were separated in batches of about 50 parts. The scanning process was conducted with 600 dpi, and the resulting images were exported in tif format. The scanning process parameters were empirically selected through initial scanning tests in order to allow for adequate representation of the monolayer part surface features.

After the images were scanned, a segmentation algorithm based on the OpenCV library was used to separate each part image individually from the scanned batches. The resulting individual images were exported in PNG format and identified as D1 for the Defect 1 condition parts, D2 for the Defect 2 condition parts, and H for the Regular condition parts. The complete monolayerFFF dataset is composed of 274 D1 images, 231 D2 images, and 271 H images. It is important to state that each image is a unique representation of an individual monolayer part surface and that no augmentation technique was used in the composition of the dataset.

C. DATASET USABILITY EVALUATION

In order to evaluate the monolayerFFF usability for CNN analysis, the well-established GoogLeNet architecture was used for classification. The training and validation were performed in the MATLAB software.

The dataset images were separated into three classes, following the three conditions. Also, the dataset images were aleatory divided into two batches: training (70% of the images), and validation (30% of the images).

For training the GoogLeNet architecture model, the selected hyperparameters were as follows: The optimizer chosen was Stochastic Gradient Descent with Momentum (SGDM). The Mini Batch Size was set to 32, indicating that 32 samples from the dataset were processed in each iteration. The training was executed for a maximum of 25 epochs, with each epoch representing a complete pass through the entire dataset. The Initial Learning Rate was 0.001 (1e-3), a critical factor influencing the speed and effectiveness of the training process.

Regarding the Initial Learning Rate and other hyperparameter values, it is important to clarify that this study primarily aims to present and describe the MonolayerFFF dataset, along with a usability evaluation using a specific CNN architecture. Therefore, a comprehensive assessment of multiple hyperparameter configurations, including variations of the learning rate, and their impact on the CNN's defect classification performance was not conducted, as this falls beyond the main scope of the present work.

It is important to mention that significant modifications were made to enhance performance and tailor it to specific requirements. Firstly, a new dropout layer was introduced. This layer, with a dropout rate of 50% was created to reduce overfitting while replacing the existing dropout. The use of this dropout rate is a common practice to increase the model's generalization on unseen data.

Next, adjustments were made to the final layers of the network to align them with the specific number of classes present in the training dataset. The number of classes was determined by counting the unique categories in the training set. Accordingly, a new fully connected layer was created, tailored to the exact number of classes. These modifications aim to improve the network's ability to learn specific features of the dataset and increase its accuracy in categorizing images into classes.

A specific test set was manufactured containing 40 class images, which were not presented to the model during the training and validation stage. This specific test set is not part of the MonolayerFFF dataset but was produced following the same printing and scanning procedures mentioned for the main dataset parts and was produced with the sole objective of evaluating the trained model classification accuracy.

IV. RESULTS AND DISCUSSION

Regarding the parts printing and scanning process, the proposed methodology was successfully applied, and the obtained MonolayerFFF dataset is available. However, it is important to point out that the alteration to the G-Code regarding the D1 condition did not have an instantaneous effect on the contour lines printing. As seen in Fig. 8 on the three examples of D1 parts, the effect on the reducing of the filament deposition begins to appear close to half of the C1, C2, and C3 contour lines right side fabrication, goes around the upper right corner, and ends at about 1/4 of the upper side fabrication. On the other hand, the result of the D2 printing condition was the appearance of a complete void of filament in the position of the R28 line, as seen in Fig. 8 on the three examples of D2 parts.

The GoogLeNet architecture's training on the monolayerFFF dataset is exemplified in the training progress chart shown in Fig. 7 and Tab. 1, with the validation accuracy peaking at 95.81%. This high level of accuracy achieved without the aid of augmentation techniques, underscores the inherent quality and diversity of the monolayerFFF dataset. Given that each image in the dataset is a unique representation of an individual monolayer part surface, the model's ability to distinguish between the three classes—D1, D2, and H—with such high accuracy is indicative of a well-tuned model and a rich dataset.

The convergence of the training accuracy with the validation accuracy suggests that the GoogLeNet model has effectively learned the defining characteristics of the monolayerFFF dataset. The absence of overfitting is particularly noteworthy, considering that no data augmentation was employed. The closely aligned loss curves for training and validation further corroborate the model's capacity to generalize well from the training data to the validation set, which is crucial for real-world applications.

The validation batch matrix represented in Fig. 9 exhibits a similar trend, with the majority of predictions falling along

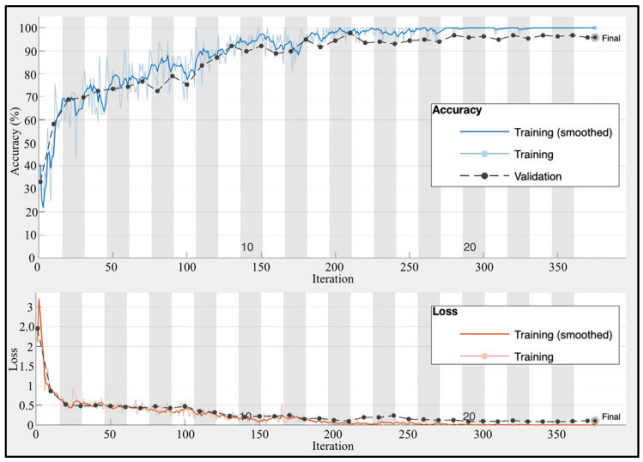

FIGURE 7. Training progress chart.

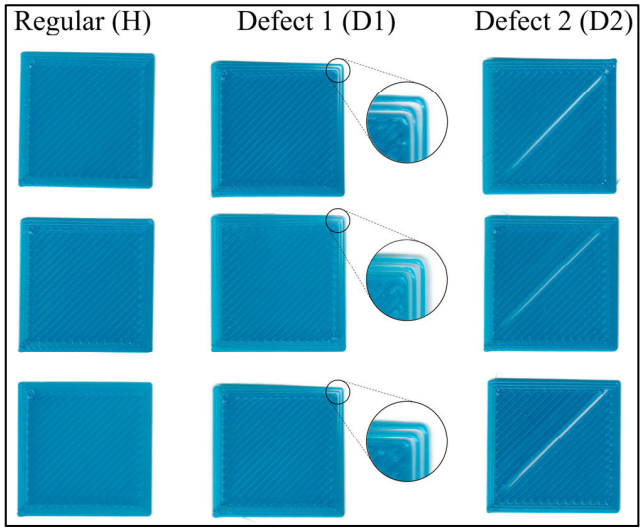

FIGURE 8. Examples of the MonolayerFFF parts classes.

TABLE 1. Training information.

Category	Item	Value
Results	Validation Accuracy	95.81%
	Training Status	Max epochs completed
Training Time	Elapsed Time	18 min 54 sec
Training Cycle	Epoch (Current / Total)	25 / 25
	Iteration (Current / Total)	375 / 375
	Iterations per Epoch	15
	Maximum Iterations	375
Validation	Frequency	Every 10 iterations
Other Information	Hardware Resource	Single CPU
	Learning Rate Schedule	Constant
	Learning Rate	0.001

the diagonal, indicating correct classifications. There are, however, some misclassifications, such as 3 instances of class D1 being classified as H, 3 instances of class D2 being classified as H, and 4 instances of H being misclassified as D2. While the sample size was smaller in the validation batch, the proportion of correct classifications remains high.

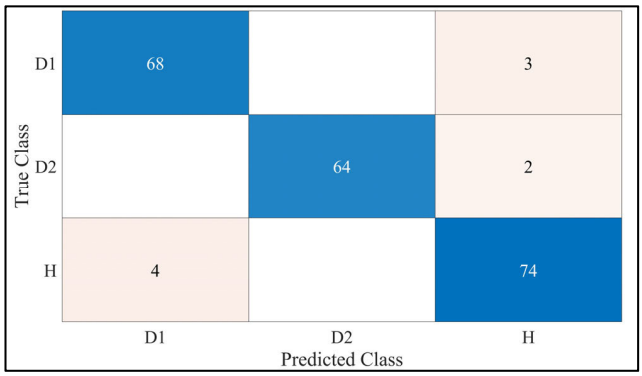

FIGURE 9. Confusion matrix for the validation batch.

As previously mentioned, the test set containing 40 samples of each class was used to evaluate the performance of the trained model. Fig. 10 shows high values along the diagonal for classes D1, D2, and H, with counts of 38, 39, and 39, respectively. This indicates a strong true positive rate, with the majority of each class being correctly identified by the model. There are a few instances of misclassification, such as 1 instance of class H being misclassified as D1, and similarly low numbers of D1 and D2 instances being misclassified. The low number of misclassifications suggests that the model has a good discriminative ability between the different classes of the monolayerFFF dataset.

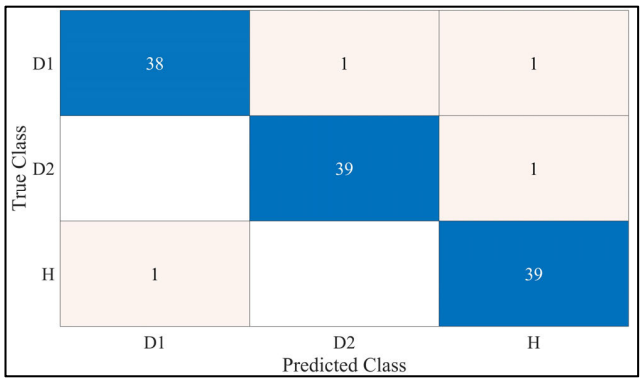

FIGURE 10. Confusion matrix for the test batch.

The GoogLeNet model's performance on the monolayerFFF dataset, as shown in the validation and test batches, highlights its high accuracy and robust classification capabilities. The minimal misclassifications across both batches not only demonstrate the model's ability to generalize effectively from the training data to unseen data but also underscore the quality and representativeness of the monolayerFFF dataset, even in the absence of data augmentation techniques. This performance consistency reinforces the model's robustness and attests to the dataset's suitability for the classification task at hand.

Further, the outcomes of this implementation underscore the monolayerFFF dataset's significant potential for advancing CNN analysis within the 3D printing and surface analysis topic.

V. CONCLUSION

This work introduced the MonolayerFFF dataset, an innovative data collection in the context of monolayer Fused Filament Fabrication (FFF) 3D printing, distinguishing itself from publicly available image datasets that focus on multilayered parts. The MonolayerFFF is unique in its approach, concentrating on monolayer parts with specific geometric variations, unlike previous datasets involving the fabrication of entire parts with significant differences in manufacturing conditions.

The MonolayerFFF dataset comprises three types of part conditions: Regular (H), without any induced defect; Defect 1 (H), featuring reduced filament deposition in specific regions of the external printing pattern; and Defect 2 (D2), characterized by filament retraction in the printing of the middle raster line. These variations are meticulously designed and documented, as demonstrated by the specific alterations in filament deposition and filament retraction, resulting in distinctive physical features in the printed parts.

Regarding the dataset usability evaluation, by applying the GoogLeNet model to the MonolayerFFF dataset, an impressive validation accuracy of 95.81% was achieved without the use of data augmentation techniques. This high accuracy reflects the dataset's quality and the model's effectiveness in distinguishing between the classes D1, D2, and H. The absence of overfitting and the aligned loss curves confirm the model's ability to generalize appropriately from the training data to the validation set, and also for the test set. The confusion matrices for both the test and validation batches show a high true positive rate and few misclassifications, underscoring the model's capability to effectively discriminate between the different classes of the MonolayerFFF dataset. This consistent performance reveals the high usability of MonolayerFFF dataset in CNN analysis for 3D printing process monitoring.

In summary, the MonolayerFFF dataset represents a significant advancement in CNN analysis for 3D printing process monitoring, thanks to its unique focus on monolayer parts and specific variations in part conditions. The success of the GoogLeNet model in accurately classifying the part conditions in the MonolayerFFF dataset highlights the dataset's quality and representativeness, even in the absence of data augmentation techniques, and points to its significant potential in real-time monitoring systems and quality assurance in the FFF additive manufacturing process.

DATA AVAILABILITY

The monolayerFFF dataset is available in the Mendeley Data repository named "*MonolayerFFF*" [27], accessible through the following link:
https://data.mendeley.com/datasets/k66f2gbgb4/2

REFERENCES

[1] S. S. Crump, "Apparatus and method for creating three-dimensional objects," U.S. Patent 5 121 329, Jun. 9, 1992.

[2] T. G. Lopes. (2021). *Detecção E Classificação De Anomalias Durante O Processo De Manufatura Aditiva Por Fusão E Deposição Por Meio De Transdutores Piezelétricos E Processamento De Sinais*. Dissertação, Universidade Estadual Paulista. Accessed: Sep. 5, 2022. [Online]. Available: https://repositorio.unesp.br/handle/11449/204399

[3] B. Shaqour, M. Abuabiah, S. Abdel-Fattah, A. Juaidi, R. Abdallah, W. Abuzaina, M. Qarout, B. Verleije, and P. Cos, "Gaining a better understanding of the extrusion process in fused filament fabrication 3D printing: A review," *Int. J. Adv. Manuf. Technol.*, vol. 114, nos. 5–6, pp. 1279–1291, May 2021, doi: 10.1007/s00170-021-06918-6.

[4] T. G. Lopes, P. R. de Aguiar, T. V. França, P. de O. C. Júnior, C. S. Soares, and Z. R. F. Antonio, "Time-domain analysis of acoustic emission signals during the first layer manufacturing in FFF process," *Eng. Proc.*, vol. 27, no. 1, p. 83, Nov. 2022, doi: 10.3390/ecsa-9-13285.

[5] T. G. Lopes, P. R. Aguiar, P. M. D. C. Monson, D. M. D'Addona, P. D. O. C. Júnior, and R. G. de Oliveira Junior, "Machine condition monitoring in FDM based on electret microphone, SVM, and neural networks," *Int. J. Adv. Manuf. Technol.*, vol. 129, nos. 3–4, pp. 1769–1786, Oct. 2023, doi: 10.1007/s00170-023-12375-0.

[6] H. Wu, Z. Yu, and Y. Wang, "A new approach for online monitoring of additive manufacturing based on acoustic emission," in *Proc. Joint MSEC-NAMRC Symposia*, New York, NY, USA, Jun. 2016, p. 8, doi: 10.1115/msec2016-8551.

[7] P. R. Aguiar, T. G. Lopes, D. M. D'Addona, R. Gotz, and T. V. França, "A study on acoustic signals from an electret microphone in 3D printing," in *Proc. 17th CIRP Conf. Intell. Comput. Manuf. Eng.*, Aug. 2024, pp. 651–655.

[8] N. Volpato, *Manufatura Aditiva: Tecnologias E Aplicações Da Impressão 3D*, vol. 1, 1st ed., São Paulo, Brazil: Blutcher, 2017.

[9] T. G. Lopes, Z. R. F. Antonio, C. S. Junior, E. L. V. Ruas, and P. R. Aguiar, "A primeira camada como indicador de qualidade do planejamento do processo de impressão 3D," in *Proc. Anais do XXVII Simpósio de Engenharia de Produção (SIMPEP)*, 2020, pp. 1–12. [Online]. Available: http://www.simpep.feb.unesp.br/anais_simpep.php?e=13

[10] H. Wu, Z. Yu, and Y. Wang, "Experimental study of the process failure diagnosis in additive manufacturing based on acoustic emission," *Measurement*, vol. 136, pp. 445–453, Mar. 2019, doi: 10.1016/j.measurement.2018.12.067.

[11] Y. Li, W. Zhao, Q. Li, T. Wang, and G. Wang, "In-situ monitoring and diagnosing for fused filament fabrication process based on vibration sensors," *Sensors*, vol. 19, no. 11, p. 2589, Jun. 2019, doi: 10.3390/s19112589.

[12] M. G. F. D. Carmo, T. G. Lopes, V. S. Bombonatti, P. R. Aguiar, and T. V. França, "Studying the defects and geometric anomalies on monolayer parts obtained via the fused deposition modeling process," in *Proc. 1st Int. Conf. Polym. Mater.*, Basel, Switzerland, Nov. 2020, p. 40, doi: 10.3390/cgpm2020-07159.

[13] Y. Tlegenov, G. S. Hong, and W. F. Lu, "Nozzle condition monitoring in 3D printing," *Robot. Comput.-Integr. Manuf.*, vol. 54, pp. 45–55, Dec. 2018, doi: 10.1016/j.rcim.2018.05.010.

[14] Y. Fu, A. Downey, L. Yuan, A. Pratt, and Y. Balogun, "In situ monitoring for fused filament fabrication process: A review," *Additive Manuf.*, vol. 38, Feb. 2021, Art. no. 101749, doi: 10.1016/j.addma.2020.101749.

[15] M. Pech, J. Vrchota, and J. Bednář, "Predictive maintenance and intelligent sensors in smart factory: Review," *Sensors*, vol. 21, no. 4, p. 1470, Feb. 2021, doi: 10.3390/s21041470.

[16] R. M. Scheffel, A. A. Fröhlich, and M. Silvestri, "Automated fault detection for additive manufacturing using vibration sensors," *Int. J. Comput. Integr. Manuf.*, vol. 34, no. 5, pp. 500–514, May 2021, doi: 10.1080/0951192x.2021.1901316.

[17] K. Xu, J. Lyu, and S. Manoochehri, "In situ process monitoring using acoustic emission and laser scanning techniques based on machine learning models," *J. Manuf. Processes*, vol. 84, pp. 357–374, Dec. 2022, doi: 10.1016/j.jmapro.2022.10.002.

[18] A. Saluja, J. Xie, and K. Fayazbakhsh, "A closed-loop in-process warping detection system for fused filament fabrication using convolutional neural networks," *J. Manuf. Processes*, vol. 58, pp. 407–415, Oct. 2020, doi: 10.1016/j.jmapro.2020.08.036.

[19] R. Yamashita, M. Nishio, R. K. G. Do, and K. Togashi, "Convolutional neural networks: An overview and application in radiology," *Insights into Imag.*, vol. 9, no. 4, pp. 611–629, Aug. 2018, doi: 10.1007/s13244-018-0639-9.
[20] Z. Jin, Z. Zhang, and G. X. Gu, "Autonomous in-situ correction of fused deposition modeling printers using computer vision and deep learning," *Manuf. Lett.*, vol. 22, pp. 11–15, Oct. 2019, doi: 10.1016/j.mfglet.2019.09.005.
[21] W. Al-Dhabyani, M. Gomaa, H. Khaled, and A. Fahmy, "Dataset of breast ultrasound images," *Data Brief*, vol. 28, Feb. 2020, Art. no. 104863, doi: 10.1016/j.dib.2019.104863.
[22] L. Yin, Y. Liu, M. Pei, J. Li, M. Wu, and Y. Jia, "Laryngoscope8: Laryngeal image dataset and classification of laryngeal disease based on attention mechanism," *Pattern Recognit. Lett.*, vol. 150, pp. 207–213, Oct. 2021, doi: 10.1016/j.patrec.2021.06.034.
[23] C. Luo, L. Yu, E. Yang, H. Zhou, and P. Ren, "A benchmark image dataset for industrial tools," *Pattern Recognit. Lett.*, vol. 125, pp. 341–348, Jul. 2019, doi: 10.1016/j.patrec.2019.05.011.
[24] J. Lyu, J. Akhavan, and S. Manoochehri, "Image-based dataset of artifact surfaces fabricated by additive manufacturing with applications in machine learning," *Data Brief*, vol. 41, Apr. 2022, Art. no. 107852, doi: 10.1016/j.dib.2022.107852.
[25] F. Caltanissetta, L. Bertoli, and B. M. Colosimo, "In-situ monitoring of image texturing via random forests and clustering with applications to additive manufacturing," *IISE Trans.*, vol. 56, no. 10, pp. 1–15, Oct. 2024, doi: 10.1080/24725854.2023.2257255.
[26] S. S. Avro, S. M. A. Rahman, T.-L. B. Tseng, and M. F. Rahman, "A deep learning framework for automated anomaly detection and localization in fused filament fabrication," *Manuf. Lett.*, vol. 41, pp. 1526–1534, Oct. 2024, doi: 10.1016/j.mfglet.2024.09.179.
[27] T. G. Lopes, P. M. C. Monson, P. R. Aguiar, D. M. Daddona, and P. O. C. Junior, Jul. 21, 2025, "MonolayerFFF," *Mendeley Data: V2*, doi: 10.17632/k66f2gbgb4.2.

THIAGO G. LOPES received the B.S. degree in control and automation engineering from the Centro Universitário de Lins, Lins, in 2018, and the M.S. and Ph.D. degrees in electrical engineering from São Paulo State University, Bauru, in 2021 and 2024, respectively. He is currently a Postdoctoral Researcher with the University of São Paulo (USP), São Carlos, Brazil; a Doctorate Professor with the Penápolis Educational Foundation (FUNEPE), Penápolis, Brazil; and the EBTT Professor under temporary contract (substitute) with Brazilian Federal Institute of Education, Science and Technology of São Paulo (IFSP), Birigui Campus, Birigui, Brazil.

PAULO M. C. MONSON received the bachelor's degree in industrial automation from the Faculty of Technology of the State of São Paulo (FATEC), São Paulo, Brazil, in 2021, and the M.Sc. degree in electrical engineering with Sao Paulo State University (UNESP), Bauru, Brazil, in 2023. He is currently pursuing the Ph.D. degree in electrical engineering with the University of São Paulo (USP), São Carlos, Brazil. He is a Researcher with the Laboratory of Industrial Automation (LAI). His research interests include digital signal processing, computer vision, and deep learning.

PAULO R. AGUIAR received the degree in electrical engineering from São Paulo State University (UNESP), in 1985, and the Ph.D. degree from the University of São Paulo (USP), in 1998. From 1998 to 1999, he was a Postdoctoral Fellow with the University of Connecticut, Storrs, CT, USA. He is currently leading the Data Acquisition and Signal Processing Laboratory. His current research interests include the monitoring of the grinding process, digital signal processing, and the industrial application of artificial neural networks and fuzzy logic.

DORIANA M. D'ADDONA received the M.Sc. degree in electronics engineering and the Ph.D. degree in intelligent technology and systems for production automation from the University of Naples Federico II, Naples, Italy, in 1999 and 2003, respectively.

From 2004 to 2006, she was a Postdoctoral Fellow Contract with Intelligent Computation for Manufacturing Technology and Systems. She is currently an Assistant Professor with the Department of Chemical, Materials and Industrial Production Engineering, University of Naples Federico II. Her current research interests include manufacturing processes and automation and intelligent computation for manufacturing technology and systems.

PEDRO O. C. JÚNIOR (Senior Member, IEEE) received the M.Sc. and Ph.D. degrees in electrical engineering from São Paulo State University, Bauru, Brazil, in 2016 and 2020, respectively. He is currently an Assistant Professor with São Carlos School of Engineering, University of São Paulo, São Carlos, Brazil, where he coordinates the Smart Sensing and Data Analysis Research Group and works in the areas of sensor systems, digital signal processing, acoustic emission, fault diagnosis, data analysis, and industrial automation. He is an Associate Editor of IEEE TRANSACTIONS ON INSTRUMENTATION AND MEASUREMENT.

Coordenação de Aperfeiçoamento de Pessoal de Nível Superior (CAPES) - ROR identifier: 00x0ma614